

# Giant Magellan Telescope Laser Tomography Adaptive Optics Simulation Documentation

Research School of Astronomy and Astrophysics  
ANU College of Physical and Mathematical Sciences  
The Australian National University

ANU-AO-

## Revision History

Version No.	Author & Date	Approval & Date	Description
0.1	P. Piatrou & R. Conan, December 7, 2011		Draft

## Contents

<b>1</b>	<b>Purpose</b>	<b>4</b>
<b>2</b>	<b>Applicable Documents</b>	<b>4</b>
<b>3</b>	<b>Modeling of atmospheric turbulence</b>	<b>5</b>
3.1	Nomenclature . . . . .	5
3.2	Atmospheric turbulence statistics for the GMT location . . . . .	5
3.3	Random phase screen generation . . . . .	5
<b>4</b>	<b>Laser guide star modeling</b>	<b>6</b>
4.1	Nomenclature . . . . .	6
4.2	LGS propagation geometry . . . . .	7
4.3	Finding LGS spot elongation and orientation on the detector . . . . .	8
4.4	Free-space propagation from LGS to telescope entrance pupil . . . . .	9
4.5	Geometrical optics propagation through atmosphere . . . . .	9
4.5.1	Turbulence layers are perpendicular to the telescope optical axis. . . . .	10
4.5.2	Turbulence layers are parallel to the ground. . . . .	10
4.6	Point source distribution in the LGS . . . . .	11
4.7	Return flux in the entrance pupil . . . . .	11
<b>5</b>	<b>Shack-Hartmann Wavefront sensor modeling</b>	<b>12</b>
5.1	Nomenclature . . . . .	12
5.2	Sensor geometry . . . . .	12
5.3	Propagation from exit pupil to detector . . . . .	12
5.4	Centroiding methods . . . . .	13
5.5	Sensor noise covariance matrix . . . . .	14
5.6	Spot intensity distribution . . . . .	14
5.7	Photon noise . . . . .	15
5.8	Read-out noise . . . . .	16
<b>6</b>	<b>Deformable mirror modeling</b>	<b>17</b>
6.1	Nomenclature . . . . .	17
6.2	Deformable mirror geometry . . . . .	17
6.3	Linear model . . . . .	17
6.4	Influence functions . . . . .	17
6.5	Fitting error . . . . .	17
6.6	Internal dynamics . . . . .	17
<b>7</b>	<b>Control</b>	<b>18</b>
7.1	Linear system model and discretization . . . . .	18
7.2	Minimum Mean Square Error AO control . . . . .	18
7.2.1	DM fitting . . . . .	19
7.2.2	Phase estimation . . . . .	19
7.2.3	Joint estimation and fitting, separation principle . . . . .	20
7.2.4	Estimator for projected wavefront . . . . .	21
7.2.5	Information deficiency in the WFS model. Aliasing error. . . . .	21
7.2.6	Dynamic and closed-loop control . . . . .	21
7.3	Tomographic MMSE reconstructor . . . . .	23
7.4	GMT LTAO sub-systems . . . . .	24
7.4.1	ASM HO LGS controller algorithm . . . . .	26
7.4.2	ASM LO NGS controller algorithm . . . . .	26
7.4.3	ASM TT NGS controller algorithm . . . . .	26
7.4.4	OI DM HO LGS controller algorithm . . . . .	26

---

7.4.5	OI DM LO NGS controller algorithm . . . . .	26
7.5	GMT LTAO system fusion . . . . .	26
7.6	GMT LTAO system dynamic analysis . . . . .	26
7.7	GMT LTAO system error and robustness analysis . . . . .	26
<b>8</b>	<b>Appendix:</b>	
	Matrix derivatives	<b>27</b>
<b>9</b>	<b>Appendix:</b>	
	Basic discrete-time digital filter theory	<b>28</b>
<b>10</b>	<b>Bibliography</b>	<b>29</b>

## List of Tables

## List of Figures

1	Geometry of laser guide star propagation to the telescope entrance pupil. . . . .	7
2	Open-loop (a) and closed-loop (b) AO controller block diagrams. . . . .	22
3	Pseudo Open-Loop MMSE controller block diagram. . . . .	23

## 1 Modeling of atmospheric turbulence

### 1.1 Nomenclature

### 1.2 Atmospheric turbulence statistics for the GMT location

### 1.3 Random phase screen generation

## 2 Laser guide star modeling

Laser guide star modeling and propagation to and through telescope is viewed from algorithmic standpoint. The formulas derived herein can be used directly for coding. No approximations are used unless necessary to reduce excessive computational complexity.

The goals of this section are

1. Find wavefront phase map in the telescope entrance pupil given the following set of parameters:
  - laser launch telescope location, pointing and focus position;
  - telescope pointing;
  - position in the telescope entrance pupil.
2. Find spot elongation and orientation in the detector focal plane.
3. Find photon fluxes through the wavefront sensor subapertures.

### 2.1 Nomenclature

*g*-system - “global” or “laboratory” coordinate system with respect to which all other coordinates and coordinate systems are defined. *Z*-axis is along the telescope optical axis at zenith position pointing towards the sky (Fig. 1).

*t*-system - “telescope” coordinate system such that its *z*-axis is always along the telescope optical axis for any zenith or azimuth angle.

*l*-system - “laser launch telescope” coordinate system such that its *z*-axis is always along the laser launch telescope optical axis.

$(\mathbf{o}, \mathcal{R})_b^a$  - the “orientation pair” consisting of the origin coordinate vector  $\mathbf{o}$  and rotation matrix  $\mathcal{R}$  to specify coordinate transformation from coordinate system *a* to coordinate system *b* or, in other words, origin and ort coordinates of *b*-system written in *a*-system.

$h_0, h_+, h_-$  - median, upper and lower altitudes of the Na layer, [m].

$\text{Eu}(\alpha, \beta, \gamma)$  - coordinate rotation by Euler angles  $\alpha, \beta, \gamma$ , [rad].

$\beta_t^g$  - zenith angle of telescope with respect to *g*-system, [rad].

$\beta_l^t$  - zenith angle of the  $l^{th}$  LGS with respect to *t*-system, [rad].

$\mathbf{r}_l^t$  - coordinates of  $l^{th}$  Laser Launch Telescope (LLT) projected to the telescope Entrance Pupil (EnP), [m].

$\mathbf{r}_p^t$  - coordinates of  $p^{th}$  point in the EnP grid, [m].

$\mathbf{r}_{li}^l$  - coordinates of  $i^{th}$  point source in the  $l^{th}$  Laser Guide Star (LGS), in *l*-system, [m].

$r_{lip}$  - distance from  $i^{th}$  point source in the  $l^{th}$  LGS to  $p^{th}$  point in EnP, [m].

$\Phi_{li}$  - photon flux from  $i^{th}$  point source belonging to  $l^{th}$  LGS, [photons].

$s^{\text{Na}}$  - sodium coupling efficiency,  $[(\text{photons m}^2)/(\text{s W atom})]$ .

$C^{\text{Na}}$  - sodium abundance,  $[\text{atoms/m}^2]$ .

$\lambda$  - wavelength,  $[\text{m}]$ .

$k = \frac{2\pi}{\lambda}$  - wave number,  $[\text{rad/m}]$ .

## 2.2 LGS propagation geometry

Geometry of the LGS propagation problem is presented on Fig. 1. The parameters describing the problem are chosen to 1) be close to the ones directly measurable on real telescope, 2) be able to describe quite general situation.

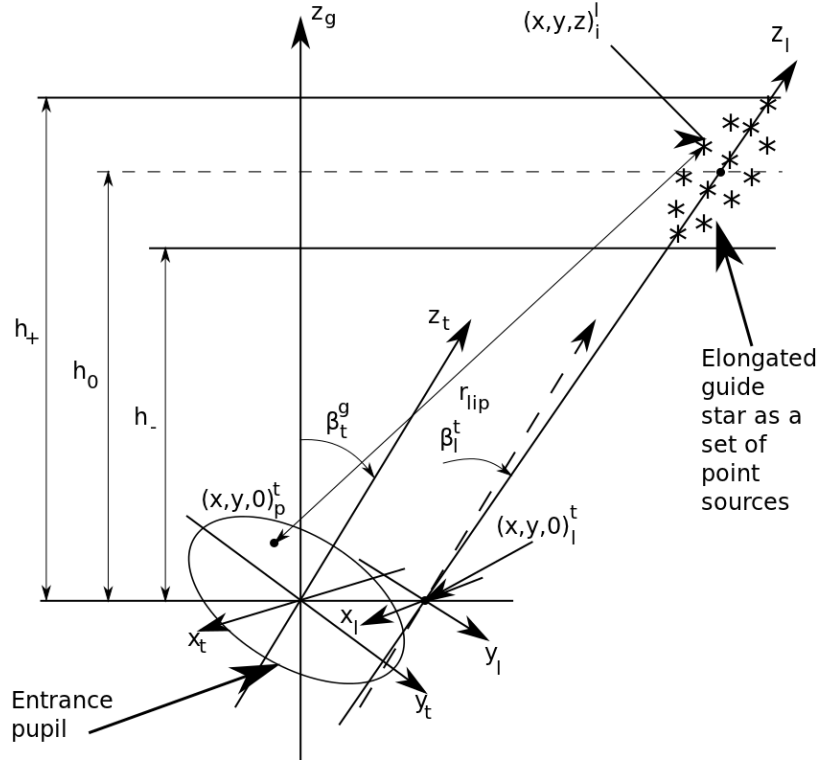


Figure 1: Geometry of laser guide star propagation to the telescope entrance pupil.

Three coordinate systems are involved:

1. Global or  $g$ -system is the Cartesian coordinate system with respect to which all other coordinate systems are defined. The orientation pair  $(\mathbf{o}, \mathcal{R})_g^0$  for this system is just  $(\mathbf{0}, \mathcal{I})$ .
2. Telescope or  $t$ -system is the local Cartesian coordinate system rotating with respect to the  $g$ -system such that the  $t$ -system  $z$ -axis is always along the telescope optical axis. The orientation pair  $(\mathbf{o}, \mathcal{R})_t^g$  for this system describes the telescope pointing. If we assume that at zenith pointing the  $t$ -system coincides with the  $g$ -system, then

$$\mathbf{o}_t^g = \mathbf{o}_g^0 = \mathbf{0}, \quad (2.2.1)$$

$$\mathcal{R}_t^g = \text{Eu}(\alpha_t^g, \beta_t^g, 0), \quad (2.2.2)$$

where Euler angles  $\alpha_t^g, \beta_t^g$  have meaning of the telescope azimuth and zenith angles measured with respect to the  $g$ -system (note the  $g$  superscript). The standard Euler rotation is

$$\text{Eu}(\alpha, \beta, \gamma) = \mathcal{A}_z(\alpha)\mathcal{A}_y(\beta)\mathcal{A}_z(\gamma), \quad (2.2.3)$$

$$\mathcal{A}_z(\alpha) = \begin{bmatrix} \cos \alpha & -\sin \alpha & 0 \\ \sin \alpha & \cos \alpha & 0 \\ 0 & 0 & 1 \end{bmatrix},$$

$$\mathcal{A}_y(\beta) = \begin{bmatrix} \cos \beta & 0 & \sin \beta \\ 0 & 1 & 0 \\ -\sin \beta & 0 & \cos \beta \end{bmatrix}.$$

Coordinates of point  $p$  in the entrance pupil given in  $t$ -system are  $[x, y, 0]_p^t = \mathbf{r}_p^t$ .

3. Laser launch telescope or  $l$ -system is a local Cartesian coordinate system chosen such that its  $z$ -axis is always along the optical axis of the LLT. This system is naturally defined with respect to the  $t$ -system because the LLT is mounted on the moving main telescope mount:

$$(\mathbf{o}, \mathcal{R})_l^t = ([x, y, 0]_l^t, \text{Eu}(\alpha_l^t, \beta_l^t, 0)), \quad (2.2.4)$$

where  $[x, y, 0]_l^t = \mathbf{r}_l^t$  are the  $l^{\text{th}}$  LLT location in  $t$ -system (pupil coordinates),  $\alpha_l^t, \beta_l^t$  are the azimuth and zenith angles of the LLT orientation with respect to the main telescope optical axis. Note that, for simplicity, we count one LGS per one LLT. In reality one LLT of GMT will generate a pair of LGSs. To account for this we simply assume that there are two differently oriented virtual LLTs at the location of one real LLT.

The LGS is modeled as a combination of the point sources (PS) distributed within the Na layer. Coordinates  $\mathbf{r}_{li}^l$ ,  $l = 1, \dots, \#LLT$ ,  $i = 1, \dots, \#PS$  of the sources are given in the  $l$ -system.

Given orientation pair  $(\mathbf{o}, \mathcal{R})_b^a$  defining  $b$ -system coordinates with respect to  $a$ -system coordinates, the transformation of coordinates written in  $b$ -system into the same coordinates written in  $a$ -system is the *direct affine transform*:

$$\mathbf{r}^a = \mathcal{R}_b^a \mathbf{r}^b + \mathbf{o}_b^a. \quad (2.2.5)$$

Correspondingly, the *inverse affine transform* gives the coordinates written in  $b$ -system from the ones written in  $a$ -system:

$$\mathbf{r}^b = (\mathcal{R}_b^a)^T (\mathbf{r}^a - \mathbf{o}_b^a). \quad (2.2.6)$$

## 2.3 Finding LGS spot elongation and orientation on the detector

An important geometrical calculation needed for the theoretical evaluation of the detector noise covariance matrix is to find the parameters of the elongated LGS image in the detector focal plane.

Let a LGS is produced as a light-emitting column of length  $L$  inside the Na layer. We need to find the length of its image in the Shack-Hartmann WFS focal plane behind a lenslet with location  $\mathbf{r}_l^t$  (in the  $t$ -system) projected on the telescope entrance pupil and the image orientation with respect to the detector pixel grid. Let the beginning and end of the LGS light column have  $t$ -system coordinates  $\mathbf{r}_1^t$  and  $\mathbf{r}_2^t$ , respectively. Consider vectors  $\mathbf{r}_{1l}^t = \mathbf{r}_1^t - \mathbf{r}_l^t$  and  $\mathbf{r}_{2l}^t = \mathbf{r}_2^t - \mathbf{r}_l^t$ . Then, up to a scaling factor and a possible mirror flip, the LGS image on the detector is determined by a  $(\varepsilon, \theta)$ -pair, where  $\varepsilon$  is the angular size of the LGS column as seen from the lenslet center  $\mathbf{r}_l^t$ , that is, the angle between vectors  $\mathbf{r}_{1l}^t$  and  $\mathbf{r}_{2l}^t$ , and  $\theta$  is the angle between the  $t$ -system  $x$ -axis and the line of intersection of the  $t$ -system  $xy$ -plane and the plane made by vectors  $\mathbf{r}_{1l}^t$  and  $\mathbf{r}_{2l}^t$ . Vectors  $\mathbf{r}_{1,2}$  are most conveniently definable in the  $l$ -system, where

$$\mathbf{r}_{1,2}^l = [00z_{1,2}^l]^T. \quad (2.3.1)$$

The transformation to  $t$ -system is

$$\mathbf{r}_{1,2}^t = \mathcal{R}_l^t \mathbf{r}_{1,2}^l + \mathbf{o}_l^t. \quad (2.3.2)$$

Using scalar and vector products we get

$$\hat{\mathbf{r}}_{1,2}^t = \frac{\mathbf{r}_{1,2}^t}{|\mathbf{r}_{1,2}^t|}, \quad (2.3.3)$$

$$\cos \varepsilon = \hat{\mathbf{r}}_1^t \cdot \hat{\mathbf{r}}_2^t, \quad (2.3.4)$$

$$\mathbf{p}_{12}^t = \hat{\mathbf{r}}_1^t \times \hat{\mathbf{r}}_2^t, \quad (2.3.5)$$

$$\sin \varepsilon = |\mathbf{p}_{12}^t|, \quad (2.3.6)$$

$$\hat{\mathbf{p}}_{12}^t = \frac{\mathbf{p}_{12}^t}{\sin \varepsilon}, \quad (2.3.7)$$

$$\hat{\mathbf{x}}^t = [1 \ 0 \ 0]^T, \quad (2.3.8)$$

$$\cos \theta = \hat{\mathbf{x}}^t \cdot \hat{\mathbf{p}}_{12}^t, \quad (2.3.9)$$

$$\sin \theta = |\hat{\mathbf{x}}^t \times \hat{\mathbf{p}}_{12}^t|. \quad (2.3.10)$$

Note that, since  $\varepsilon$  is very small, in order to preserve accuracy, all calculations need to be done in double precision.

## 2.4 Free-space propagation from LGS to telescope entrance pupil

The electric field  $E$  from the LGS on the telescope entrance pupil is the superposition of spherical waves emitted from each point source (PS) that makes the elongated laser guide star spot in the Na layer:

$$E_{lp} = \sum_{i=1}^{\#PS} w_{li} \frac{\exp(ikr_{lip})}{r_{lip}}, \quad (2.4.1)$$

where  $w_{li}$  is the weight describing relative intensity of the  $i^{th}$  PS of the  $l^{th}$  LGS,  $r_{lip}$  is the distance from the  $i^{th}$  PS of the  $l^{th}$  LGS to  $p^{th}$  point in the telescope entrance pupil. This distance is easily found through the affine transform:

$$\begin{aligned} \mathbf{r}_{li}^t &= \mathcal{R}_l^t \mathbf{r}_{li}^l + \mathbf{o}_l^t, \\ r_{lip} &= |\mathbf{r}_{li}^t - \mathbf{r}_p^t|. \end{aligned} \quad (2.4.2)$$

## 2.5 Geometrical optics propagation through atmosphere

The turbulent atmosphere on the way between an LGS and a telescope is modeled as a set of infinitely thin random *phase screens* (PS). Because of small phase perturbations caused by each layer and because the typical scale of turbulence is much larger than a wavelength the geometrical optics model for propagation through the layers is assumed. The model is based on the following postulates:

- The propagation of the electromagnetic waves is treated as propagation of *rays* that are normals to the constant phase surfaces of the waves, the *wavefronts*.
- Rays are always straight: the phase screens are weak enough for not to change direction of rays, they only add a path difference  $\delta r_{lip,j}$ :

$$\delta r_{lip,j} = \phi_{lip,j}/k, \quad j = 1, \dots, \#TL, \quad (2.5.1)$$

$$r_{lip}^{turb} = r_{lip}^{free} + \sum_{j=1}^{\#TL} \delta r_{lip,j}.$$

where  $\phi_{lip,j}$  is the phase on the  $j^{th}$  turbulent layer intersected by a ray emitting from  $i^{th}$  point source of  $l^{th}$  LGS towards  $p^{th}$  point in the entrance pupil. So, the electric field on the entrance pupil will be

$$E_{lp}^{turb} = \sum_{i=1}^{\#PS} w_{li} \frac{\exp(ikr_{lip}^{turb})}{r_{lip}^{free}}. \quad (2.5.2)$$

Thus, it is necessary to find the intersection of a ray with a turbulent layer.



### 2.5.1 Turbulence layers are perpendicular to the telescope optical axis.

Assume that the turbulence layers are chosen such that they are perpendicular to the telescope optical axis regardless of the pointing. In this case the turbulence strength depends on the azimuth angle  $\beta_t^g$ , namely,

$$C_n^2(\beta_t^g) = \frac{C_n^2(0)}{\cos \beta_t^g}. \quad (2.5.3)$$

Simple geometrical analysis gives for the relationship between the pupil and turbulence layer coordinates:

$$\mathbf{r}_{lip,j}^t = \frac{h_j}{z_{li}^t} \begin{bmatrix} x_p^t \\ y_p^t \\ 0 \end{bmatrix} + \left(1 - \frac{h_j}{z_{li}^t}\right) \begin{bmatrix} x_{li}^t \\ y_{li}^t \\ 0 \end{bmatrix}, \quad (2.5.4)$$

$$\mathbf{r}_{li}^t = \begin{bmatrix} x_{li}^t \\ y_{li}^t \\ z_{li}^t \end{bmatrix}, \quad \mathbf{r}_p^t = \begin{bmatrix} x_p^t \\ y_p^t \\ z_p^t \end{bmatrix},$$

where  $h_j$  is distance between the telescope and  $j^{th}$  phase screen along the telescope optical axis,  $\mathbf{r}_{lip,j}^t$  are xyz-coordinates in  $t$ -system of an intersection point on phase screen  $j$  for a ray emitting from  $i^{th}$  point source of  $l^{th}$  LGS with  $t$ -coordinates  $\mathbf{r}_{li}^t$  and passing through  $p^{th}$  point in telescope entrance pupil with  $t$ -coordinates  $\mathbf{r}_p^t$ .

### 2.5.2 Turbulence layers are parallel to the ground.

Assume that the layers are parallel to the ground, i.e. perpendicular to the  $g$ -system's  $z$ -axis, and have altitudes  $h_j$ ,  $j = 1, \dots, \#PS$ . In this case the turbulence  $C_n^2$  profile is not altered with the zenith angle. Direct ray tracing technique is used to find intersection with a turbulence layer.

Coordinates of a ray can be described through the parametric equation:

$$\mathbf{r}(t) = \mathbf{i}t + \mathbf{r}_0, \quad (2.5.5)$$

where  $\mathbf{r}_0$  is the ray origin (position of the light-emitting source),  $\mathbf{i}$ ,  $|\mathbf{i}| = 1$  is the ray direction vector,  $t$  is the ray path length. In the case of propagation path shown of Fig. 1

$$\mathbf{r}_0^l = \mathbf{r}_{li}^l,$$

where  $\mathbf{r}_0$  is given in  $l$ -system,

$$\mathbf{i}^t = \frac{\mathbf{r}_p^t - \mathbf{r}_{li}^t}{|\mathbf{r}_p^t - \mathbf{r}_{li}^t|},$$

where  $\mathbf{i}$  is given in  $t$ -system. Since the turbulent layers are most conveniently defined in the  $g$ -system, the ray coordinates need to be transformed into  $g$ -system:

$$\mathbf{r}_0^t = \mathcal{R}_i^t \mathbf{r}_0^l + \mathbf{o}_i^t, \quad (2.5.6)$$

$$\mathbf{i}^t = \frac{\mathbf{r}_p^t - \mathbf{r}_0^t}{|\mathbf{r}_p^t - \mathbf{r}_0^t|},$$

$$\mathbf{r}_0^g = \mathcal{R}_t^g \mathbf{r}_0^t + \mathbf{o}_t^g,$$

$$\mathbf{i}^g = \mathcal{R}_i^g \mathbf{i}^t.$$

The coordinates of ray intersection with turbulent layer are found by equating  $z$ -coordinate of a ray to the layer altitude:

$$t = \frac{h_j - r_{0z}^g}{i_z^g}, \quad (2.5.7)$$

$$\mathbf{r}_{lip,j}^g = \mathbf{i}^g t + \mathbf{r}_0^g,$$

where  $x$ - and  $y$ -coordinates of the  $\mathbf{r}_{lip,j}^g$ -vector are used to find the phase  $\phi^{turb}(\mathbf{r}_{lip,j}^g) = k\delta r_{lip,j}^{turb}(\mathbf{r}_{lip,j}^g)$  on the phase screen corresponding to the ray intersection and substitute it to Eq. (4.5.2).

## 2.6 Point source distribution in the LGS

TBC

The positions  $\mathbf{r}_{li}^l$  and weights  $w_{li}$  of point sources making each LGS are found from superposition of the intensity distribution of the laser radiation forward-propagated through atmosphere to the Na layer and the vertical distribution of the Na density. A possible operation flow for defining the LGS distribution is the following:

1. Define a 3D mesh covering a part of the Na layer penetrated by the laser radiation. Each cell of this mesh is an elementary volume for which amount of laser flux is assigned.
2. Center of each 3D mesh cell is the candidate location of the LGS point source. If flux through the cell exceeds a threshold, a point source is assigned for this cell.
3. For each mesh cell for which a point source is assigned multiply the cell flux by Na density at the cell center taken from the Na vertical profile. Find relative distribution of the return flux, which is the source weights  $\{w_{li}\}_{i=1}^{\#PS}$ :

$$w_{li} = \frac{\Phi_{li} C_{li}^{\text{Na}}}{\sum_{i=1}^{\#PS} \Phi_{li} C_{li}^{\text{Na}}}, \quad i = 1, \dots, \#PS \quad (2.6.1)$$

where  $\{\Phi_{li}\}_{i=1}^{\#PS}$  are the cell fluxes,  $\{C_{li}^{\text{Na}}\}_{i=1}^{\#PS}$  are the Na abundances at the cell locations.

## 2.7 Return flux in the entrance pupil

The photon flux returning from each LGS point source is considered uniformly distributed over the spherical surface of the wavefront. Since the solid angle  $\Omega$  at which the telescope is seen from the source is typically very small, the variation of  $r_{lip}^{free}$  in the denominator of Eq. (4.5.2) over the pupil can be neglected. Thus, the fraction of energy emitting from a point source that passes through the telescope entrance pupil is

$$\frac{\Omega}{4\pi} = \frac{1}{4\pi} \frac{A_p}{|\mathbf{r}_{li}^t|^2 \cos^2 \beta_{li}^t}, \quad (2.7.1)$$

where  $A_p$  is the pupil area,  $|\mathbf{r}_{li}^t|$  is the distance from pupil center to the point source,  $\beta_{li}^t$  is the angle between the telescope optical axis and the direction to the point source as seen from the pupil center,

$$\cos \beta_{li}^t = \left( \frac{\mathbf{r}_{li}^t}{|\mathbf{r}_{li}^t|} \right)_z. \quad (2.7.2)$$

The photon flux into the entrance pupil from a point source is

$$\Phi_{li} = \tau T_{AOS} \frac{T_{ATM}}{\cos \beta_{li}^g} s^{\text{Na}} C^{\text{Na}} P_l w_{li} \frac{\Omega}{4\pi}, \quad [\text{photons}], \quad (2.7.3)$$

where

Exposure time	:	$\tau$	= 2 ms,
Atmosphere transmittance	:	$T_{ATM}$	= 0.89,
AO system transmittance	:	$T_{AOS}$	= 0.448,
Sodium coupling efficiency	:	$s^{\text{Na}}$	= 130 (photons m <sup>2</sup> )/(s W atom),
Sodium abundance	:	$C^{\text{Na}}$	= 2.1 × 10 <sup>13</sup> atoms/m <sup>2</sup> ,
Laser power per LGS	:	$P_l$	= 20 W,

$\beta_{li}^g$  is the angle between zenith direction and the point source direction as viewed from the entrance pupil center.

The fluxes from all point sources are later summed on the detector.

### 3 Shack-Hartmann Wavefront sensor modeling

#### 3.1 Nomenclature

$\mathbf{s} = (s_x, s_y)$  - vector of xy-slope measurements read from one Shack-Hartmann sensor subaperture, [m or pixels].

$I(x, y)$  - intensity distribution in the detector focal plane, [].

$\langle \mathbf{s} \mathbf{s}^T \rangle - \langle \mathbf{s} \rangle \langle \mathbf{s} \rangle^T$  - covariance matrix of the xy-slope measurements, [m<sup>2</sup> or pixel<sup>2</sup>].

$A$  - area of subaperture, [m<sup>2</sup>].

$p$  - detector pixel size, [m].

$n_{ph}$  - number of photons passed through a subaperture, [].

$\sigma_e$  - readout noise, [electrons/pixel].

$f_L$  - lenslet focal distance, [m]

$\Gamma_L$  - angular magnification in the detector exit pupil, [].

$\varepsilon_{Na}$  - angular fwhm size of Na LGS projected to sky as seen from a subaperture, [rad].

$\varepsilon_0$  - angular fwhm size of a point source projected to sky as seen from a subaperture, [rad].

$\theta_e$  - orientation angle of the elongated spot on the detector, [rad].

#### 3.2 Sensor geometry

TBD

#### 3.3 Propagation from exit pupil to detector

The sampling of the pupil is derived from the sampling in the WFS detector focal plane. If  $n_d$  is the number of samples across each spot on the detector and the fwhm of the diffraction limited spot is sampled with  $k$  pixels, then the pupil sampling is  $2Nn_d/k = Nn$ , where  $N$  is number of subapertures across the pupil diameter,  $n$  is number of pixels across a subaperture diameter. It is required that either  $k$  or  $1/k$  is an integer and that  $k \leq 2$ . It is worth nothing that a field stop the size of a subaperture field-of-view is assumed. The pixel scale and the field-of-view are given by  $\lambda/dk$  and  $n_d\lambda/dk$ , respectively, with  $\lambda$  the wavefront sensing wavelength and  $d$  the lenslet pitch.

The Shack-Hartmann wavefront sensor (SH-WFS) model

1. the telescope pupil  $\Pi$  is cut in  $N \times N$  square pieces of  $n \times n$  pixels corresponding to the  $N \times N$  lenslet array, for the lenslet  $(k, l)$  this is

$$a_{kl} = \Pi[kn, \dots, (k+1)n-1][ln, \dots, l(n+1)-1] \quad k, l = 0, \dots, N-1,$$

2. each square array is multiplied by a complex phase ramp to keep the spot at the center of the array in the free aberration case,

$$a'_{kl}(i, j) = a_{kl}(i, j) \exp(\iota \pi (i + j)(n - 1)/n') \quad i, j = 0, \dots, n - 1$$

with  $n' = 2n$  if  $n$  is even or  $n' = 2n + 1$  if  $n$  is odd and  $\iota = \sqrt{-1}$ ,

3. each square array is padded with zeros in both directions up to  $n'$ ,

$$a'_{kl}[n, \dots, n' - 1][n, \dots, n' - 1] = 0,$$

4. a discrete Fourier transform is performed on each zero-padded array,

$$\tilde{a}'_{kl} = DFT \{a'_{kl}\},$$

5. each resulting array is reduced to half its size,

$$\tilde{a}_{kl} = \tilde{a}'_{kl}[0, \dots, n - 1][0, \dots, n - 1],$$

6. the spot intensities are computed from the squared modulus of the reduced arrays,

$$b_{kl} = |\tilde{a}_{kl}|^2,$$

7. if needed i.e.  $k < 2$ , the intensity map are binned to the detector array size,

$$b'_{kl}(k, l) = \sum_{i=kn_d}^{(k+1)n_d-1} \sum_{j=ln_d}^{(l+1)n_d-1} b_{kl}(i, j) \quad k, l = 0, \dots, n_d - 1$$

### 3.4 Centroiding methods

The four spot centroiding methods are considered for the GMT LTAO Shack-Hartmann sensors:

1. *Center of Gravity*:

$$\begin{bmatrix} s_x \\ s_y \end{bmatrix} = \frac{1}{\sum_{xy} I(x, y)} \sum_{xy} \begin{bmatrix} x \\ y \end{bmatrix} I(x, y), \quad (3.4.1)$$

where  $\mathbf{s} = (s_x, s_y)$  is the slope readout from the spot,  $I(x, y)$  is the intensity distribution read out from detector pixels, summation is done over the pixels in the area occupied by a single spot.

2. *Weighted Center of Gravity* is the Center of Gravity algorithm applied to image  $I(x, y)I_0(x, y)$ , where  $I_0(x, y)$  is a *reference image*.
3. *Correlation* algorithm finds spot position as that of maximum of the correlation function

$$C(\mathbf{s}) = \sum_{xy} I(x, y)I_0(x - s_x, y - s_y), \quad (3.4.2)$$

where  $I_0(x, y)$  is a reference image.

4. *Quad cell* centroiding algorithm is used in the tip/tilt WFS, which has 4 pixels per spot. The quad cell readout is

$$\begin{aligned} s_x &= \frac{1}{\sum_{i=1}^4 I_i} (I_1 + I_2 - I_3 - I_4), \\ s_y &= \frac{1}{\sum_{i=1}^4 I_i} (I_1 + I_3 - I_2 - I_4), \end{aligned} \quad (3.4.3)$$

where  $\{I_i\}_{i=1}^4$  are the four intensity reads from the quad cell pixels.

Discussion of these centroiding approaches is given in Ref. [1].

### 3.5 Sensor noise covariance matrix

This section describes the derivation of the noise covariance matrix for a SH-WFS with a  $N_L \times N_L$  lenslet array paving a telescope pupil of diameter  $D$ . The spots of the SH-WFS are assumed to be seeing limited i.e.  $r_0 < D/N_L$ ,  $r_0$  is the Fried parameter. Thus, the projected to sky angular size of the spot formed by a lenslet is  $\varepsilon_0 = \lambda/r_0$ ,  $\lambda$  is the WFS operational wavelength. The spot elongation due to elongated LGS is characterized by the  $(\varepsilon_{Na}, \theta_e)$ -pair of the fwhm angular size along the **Na** LGS elongation direction and the elongation orientation angle. Both these parameters depend on the mutual orientation lenslet and the LLT, altitude and thickness of the **Na** layer, and the LLT pointing. The calculation of the  $(\varepsilon_{Na}, \theta_e)$ -pair is described in Section 4.3.

The spot intensity profile due to the LGS is assumed to be Gaussian with elliptical cross section and the long ellipse axis is rotated by angle  $\theta_e$  with respect to the camera focal plane xy-coordinates:

$$I_S(x, y) = \frac{n_{ph}}{2\pi\sigma_x\sigma_y} \exp\left(-\frac{x'^2 + y'^2}{2\sigma_x\sigma_y}\right), \quad (3.5.1)$$

where subscript  $S$  stands for the star image distribution,  $n_{ph}$  is the photon flux through the sub-aperture,

$$x' = x \cos(\theta_e) - y \sin(\theta_e), \quad (3.5.2)$$

$$y' = x \sin(\theta_e) + y \cos(\theta_e), \quad (3.5.3)$$

$\sigma_x$  and  $\sigma_y$  are related to the fwhm of the non-elongated and elongated spot, respectively, as

$$\varepsilon_{x,y} = 2\sqrt{2 \ln(2)}\sigma_{x,y}, \quad (3.5.4)$$

$$\varepsilon_{x,y} = f_L \Gamma_L \varepsilon_{0,Na}, \quad (3.5.5)$$

where  $f_L$  is the lenslet focal distance,  $\Gamma_L$  is the angular magnification in the exit pupil where the lenslet array is located.

The spot centroid xy-readout in the lenslet focal plane in case of the *Center of Gravity* centroiding algorithm is given by

$$\mathbf{s} = \begin{bmatrix} s_x \\ s_y \end{bmatrix} = \frac{1}{\iint_A I(x, y) dx dy} \iint_A \begin{bmatrix} x \\ y \end{bmatrix} I(x, y) dx dy, \quad (3.5.6)$$

where  $I(x, y)$  is the complete intensity distribution in the spot that includes the star intensity distribution and some other additions,  $A = (D/N_L)^2$  is the lenslet area.

### 3.6 Spot intensity distribution

To proceed with computation of the spot readout covariance assumptions about the spot intensity distribution need to be made:

1. The whole intensity distribution is

$$I(x, y) = I_S(x, y) + I_B(x, y), \quad (3.6.1)$$

where  $I_S(x, y)$  is given in Eq. (5.5.1),  $I_e(x, y)$  is the background image due to sensor readout noise.

2.  $I_S(x, y)$  and  $I_B(x, y)$  are statistically independent, i.e.  $\langle I_S(x, y) I_B(x, y) \rangle = 0$ .
3.  $\langle I_B(x, y) \rangle = 0$ .
4. All the  $I_S(x, y)$  distribution energy is concentrated inside region  $A$ , so  $\iint_A I_S(x, y) dx dy \approx n_{ph} = \text{const.}$

5. The random process  $I_B(x, y)$  is ergodic, so  $0 = \langle I_B(x, y) \rangle \approx \iint_A I_B(x, y) dx dy$ , which, together with the previous assumption gives  $\iint_A I(x, y) dx dy \approx n_{ph}$ .
6. Spot cross-talk is negligible, so spots from different lenslets are statistically independent. Therefore, the full WFS readout covariance matrix is block diagonal with 2x2 blocks corresponding to each spot xy-slope covariance.
7. Pixel intensities are statistically independent, i.e.  $\langle I(x, y) I(x', y') \rangle = 0$ .

Eq. (5.5.6) due to assumptions 5, 6 simplifies to

$$\mathbf{s} = \frac{1}{n_{ph}} \iint_A \begin{bmatrix} x \\ y \end{bmatrix} I(x, y) dx dy. \quad (3.6.2)$$

The covariance of the spot centroid readouts is given by

$$\begin{aligned} & \langle \mathbf{s} \mathbf{s}^T \rangle - \langle \mathbf{s} \rangle \langle \mathbf{s}^T \rangle \\ &= \frac{1}{n_{ph}^2} \iint_A \iint_A \begin{bmatrix} x_1 x_2 & x_1 y_2 \\ y_1 x_2 & y_1 y_2 \end{bmatrix} (\langle I(x_1, y_1) I(x_2, y_2) \rangle - \langle I(x_1, y_1) \rangle \langle I(x_2, y_2) \rangle) dx_1 dy_1 dx_2 dy_2. \end{aligned} \quad (3.6.3)$$

Substituting Eq. (5.6.1) and using assumptions 2, 3, and 7 we simplify this equation to

$$\begin{aligned} & \langle \mathbf{s} \mathbf{s}^T \rangle - \langle \mathbf{s} \rangle \langle \mathbf{s}^T \rangle \\ &= \frac{1}{n_{ph}^2} \iint_A \begin{bmatrix} x^2 & xy \\ xy & y^2 \end{bmatrix} (\sigma_I^2(x, y) + \sigma_B^2) dx dy, \end{aligned} \quad (3.6.4)$$

where

$$\sigma_S^2(x, y) = \langle I_S^2(x, y) \rangle - \langle I_S(x, y) \rangle^2,$$

is the variance distribution in the star intensity distribution,

$$\sigma_B^2 = \langle I_B^2(x, y) \rangle = \text{const.}$$

is the readout noise variance. Thus the sensor readout covariance has two terms that can be treated independently.

### 3.7 Photon noise

The photon noise follows a Poisson statistics distribution with variance  $\sigma_S^2(x, y) = I_S(x, y)$ . Thus the spot centroid readouts covariance in the case of the photon noise is given by

$$\begin{aligned} & \langle \mathbf{s} \mathbf{s}^T \rangle_S - \langle \mathbf{s} \rangle_S \langle \mathbf{s}^T \rangle_S \\ &= \frac{1}{n_{ph}^2} \iint_A \begin{bmatrix} x^2 & xy \\ xy & y^2 \end{bmatrix} I_S(x, y) dx dy, \end{aligned} \quad (3.7.1)$$

where  $n_{ph}$  is the number of photons per subaperture,  $x$  and  $y$  are the coordinates in the focal plane, the intensity  $I_S(x, y)$  in the focal plane given by Eq. (5.5.1).

Substituting Eq.(5.5.1) into Eq. (5.7.1) and performing the integration leads to

$$\begin{aligned} & \langle \mathbf{s} \mathbf{s}^T \rangle_S - \langle \mathbf{s} \rangle_S \langle \mathbf{s}^T \rangle_S \\ &= \frac{1}{n_{ph}} \begin{bmatrix} \sigma_x^2 \cos^2 \theta_e + \sigma_y^2 \sin^2 \theta_e & (\sigma_x^2 - \sigma_y^2) \cos \theta_e \sin \theta_e \\ (\sigma_x^2 - \sigma_y^2) \cos \theta_e \sin \theta_e & \sigma_x^2 \sin^2 \theta_e + \sigma_y^2 \cos^2 \theta_e \end{bmatrix} \\ &= \begin{bmatrix} \sigma_{xx}^2 & \sigma_{xy}^2 \\ \sigma_{xy}^2 & \sigma_{yy}^2 \end{bmatrix}. \end{aligned} \quad (3.7.2)$$

From Eq.(5.7.2), it is obvious that covariance is null when the spots are oriented either along the x or y axis or if the fwhms of both x and y axis are the same.

### 3.8 Read-out noise

The read-out noise follows a zero-mean Gaussian distribution of variance  $\sigma_B^2 = \sigma_e^2/p^2$ , where  $\sigma_e^2$  is the number of read noise electrons squared per pixel area  $p^2$ . Since  $\sigma_B^2 = \text{const.}$  and, with assumption that  $A$  is a square lenslet, we have

$$\sigma_B^2 \iint_A xy dx dy = 0,$$

$$\iint_A x^2 dx dy = \iint_A y^2 dx dy.$$

Thus the readout noise covariance matrix is diagonal:

$$\langle \mathbf{s} \mathbf{s}^T \rangle_B = \begin{bmatrix} \sigma_{ron}^2 & 0 \\ 0 & \sigma_{ron}^2 \end{bmatrix}. \quad (3.8.1)$$

For a square lenslet of size  $d = D/N_L$  we get

$$\sigma_{ron}^2 = \left( \frac{\sigma_e}{pn_{ph}} \right)^2 \int_{-d/2}^{d/2} \int_{-d/2}^{d/2} x^2 dx dy = \frac{1}{12} \left( \frac{d^2 \sigma_e}{pn_{ph}} \right)^2 = \frac{N_d^2}{12} \left( \frac{D \sigma_e}{N_L n_{ph}} \right)^2, \quad (3.8.2)$$

$N_d$  is the total number of pixels used for computing the centroids.

Finally, the sensor readout noise covariance matrix for one lenslet is a sum of covariance matrices for photon and readout noises:

$$\langle \mathbf{s} \mathbf{s}^T \rangle_{S+B} - \langle \mathbf{s} \rangle_{S+B} \langle \mathbf{s}^T \rangle_{S+B} = \begin{bmatrix} \sigma_{xx}^2 + \sigma_{ron}^2 & \sigma_{xy} \\ \sigma_{xy} & \sigma_{yy}^2 + \sigma_{ron}^2 \end{bmatrix}. \quad (3.8.3)$$

For the whole lenslet array, the noise covariance matrix is a block diagonal with these matrices on the diagonal.

## **4 Deformable mirror modeling**

### **4.1 Nomenclature**

TBD

### **4.2 Deformable mirror geometry**

TBD

### **4.3 Linear model**

### **4.4 Influence functions**

TBD

### **4.5 Fitting error**

TBD

### **4.6 Internal dynamics**

TBD



## 5 Control

### 5.1 Linear system model and discretization

In our treatment of an AO system modeling we follow closely the “natural modeling” approach described in Refs. [2, 3]. To begin with, we consider the simplest case of a single-conjugate AO system, which is modeled through the following fundamental inputs.

1. A light source to be imaged with an AO system (the *target*) creates a continuous phase distribution  $\phi_0(x, y)$  in the telescope entrance pupil, which is the accumulated phase distortion along the path from a light source to the telescope that includes atmospheric turbulence distortion. It is supposed that the autocorrelation function  $\langle \phi_0(x_1, y_1) \phi_0(x_2, y_2) \rangle_\phi$  is known.
2. A set  $\{f_i(x, y)\}_{i=1}^{\#ACT}$  ( $\#ACT$  is the number of DM actuators) of the DM actuator influence functions projected as phase correction in the telescope entrance pupil. We will write these functions in vectorial form  $\mathbf{f}(x, y)$ . Note that, same as  $\phi(x, y)$ , these functions depend on the light source. The DM correction is assumed to be a linear combination of the influence functions:

$$\phi_{DM}(x, y) = \sum_{i=1}^{\#ACT} c_i f_i(x, y) \quad (5.1.1)$$

or

$$\phi_{DM}(x, y) = \mathbf{f}^T(x, y) \mathbf{c},$$

where  $\mathbf{c}$  is the vector of DM correction commands.

3. A wavefront sensor (WFS) accepts light from a *reference* source not in general coinciding with the target. WFS is modeled as a linear mapping of the reference wavefront  $\phi(x, y)$  in the entrance pupil to a set of sensor measurements:

$$\mathbf{s} = \mathcal{M}[\phi(x, y)], \quad (5.1.2)$$

where  $\mathcal{M}$  is a linear *measurement operator*. The *measurement equation* describing the full linear sensor model is

$$\mathbf{s} = \mathcal{M}[\phi(x, y) + \delta\phi(x, y)] + \mathbf{n}, \quad (5.1.3)$$

where  $\mathbf{n}$  is random sensor readout noise with known autocorrelation matrix  $\langle \mathbf{n} \mathbf{n}^T \rangle_n$ ,  $\delta\phi(x, y)$  is an additive aberration due to propagation from telescope entrance pupil to the exit pupil conjugate to the WFS location. We will assume for the moment that this aberration can be perfectly calibrated out, so  $\delta\phi(x, y) = 0$ .

This small set of parameters are enough to fully describe a linear model of an AO system.

### 5.2 Minimum Mean Square Error AO control

The goal of the *Minimum Mean Square Error* (MMSE) AO control is to find a command vector  $\hat{\mathbf{c}}$  such that the DM correction minimizes the target wavefront mean square phase error (*quadratic cost*) in the telescope entrance pupil

$$\langle J \rangle_{\phi, n} = \langle \|\phi_0 - \phi_{DM}\|^2 \rangle_{\phi, n}, \quad (5.2.1)$$

where Hilbert space norm

$$\|a(x, y)\|^2 = [a(x, y), a(x, y)] = \frac{1}{|A|} \int_A ds a^2(x, y), \quad (5.2.2)$$

is derived from the Hilbert space metric

$$[a(x, y), b(x, y)] = \frac{1}{|A|} \int_A ds a(x, y) b(x, y), \quad (5.2.3)$$

$A$  is the telescope entrance pupil domain (the *aperture*),  $|A|$  is the aperture area, and  $\langle \rangle_\phi$  denotes averaging over joint statistics of the input turbulent wavefront and the sensor noise. We can consider two cases of the quadratic cost minimization: 1) *DM fitting* and 2) *phase estimation*.

### 5.2.1 DM fitting

The DM fitting problem statement is: given target wavefront phase  $\phi_0(x, y)$  at the entrance pupil find the DM command vector  $\hat{\mathbf{c}}$  such that the deterministic wavefront error is minimized:

$$\hat{\mathbf{c}} = \arg \min_{\forall \mathbf{c}} \|\phi_0 - \mathbf{f}^T \mathbf{c}\|^2. \quad (5.2.4)$$

It is known from the theory of Hilbert spaces that the above equation is equivalent to

$$[\phi_0 - \mathbf{f}^T \hat{\mathbf{c}}, \mathbf{f}] = 0, \quad (5.2.5)$$

which is a form of the *orthogonality principle* stating that

the optimal fitting error is orthogonal to the subspace spanned by the influence functions.

Solving Eq. (7.2.4) or the equivalent Eq. (7.2.5) yields for the optimal control command

$$\hat{\mathbf{c}} = [\mathbf{f}, \mathbf{f}^T]^\dagger [\mathbf{f}, \phi_0], \quad (5.2.6)$$

where  $[\mathbf{f}, \mathbf{f}^T]$  is called *Gramm matrix* of the function set  $\mathbf{f}(x, y)$ ,  $^\dagger$  stands for pseudo inverse. The Gramm matrix is square and is invertible in case the influence functions  $\mathbf{f}(x, y)$  are linearly independent. Since linear independence is not guaranteed for the real DM influence functions, the filtered pseudo-inverse is used. Note that in case of pseudo-inverse the orthogonality principle does not hold exactly. This, however, is easily fixed if we redefine the influence functions as, e.g., a subset of orthogonal singular modes of the Gramm matrix with sufficiently large singular values.

The optimal *fitting error* is

$$\begin{aligned} J_c &= [\phi_0 - \mathbf{f}^T \hat{\mathbf{c}}, \phi_0 - \mathbf{f}^T \hat{\mathbf{c}}] \\ &= [\phi_0 - \mathbf{f}^T \hat{\mathbf{c}}, \phi_0] \\ &= [\phi_0, \phi_0] - [\mathbf{f}^T, \phi_0][\mathbf{f}, \mathbf{f}^T]^\dagger [\mathbf{f}, \phi_0], \end{aligned} \quad (5.2.7)$$

where we used Eqs. (7.2.5) and (7.2.6). The orthogonality principle states that the phase can be presented as a sum of two mutually orthogonal *controllable*  $\hat{\phi}_0$  and *uncontrollable*  $\check{\phi}_0$  parts

$$\phi(x, y) = \hat{\phi}_0(x, y) + \check{\phi}_0(x, y), \quad (5.2.8)$$

where

$$\hat{\phi}_0 = \mathbf{f}^T [\mathbf{f}, \mathbf{f}^T]^\dagger [\mathbf{f}, \phi_0] = \mathcal{F} \phi_0, \quad (5.2.9)$$

$$\check{\phi}_0 = \phi_0 - \mathcal{F}(\phi_0) = (\mathcal{I} - \mathcal{F}) \phi_0 \quad (5.2.10)$$

and  $\mathcal{F}, \mathcal{I} - \mathcal{F}$  are orthogonal projection operators on, respectively, *controllable* and *uncontrollable subspaces* of the influence function set  $\mathbf{f}$ . Note that the dimension of the controllable subspace is finite, so either  $\hat{\mathbf{c}}$  or  $\phi_0 = [\mathbf{f}, \phi_0]$  are the natural discrete representations for the controllable part of the wavefront phase, the only part of interest in the AO control.

### 5.2.2 Phase estimation

The phase estimation problem statement is: given sensor measurements  $\mathbf{s}$  find an estimate  $\tilde{\phi}_0(x, y)$  of the target source phase in the entrance pupil such that the mean square error is minimized over the measurement statistics, in our case, the joint turbulence and sensor noise statistics:

$$\tilde{\phi}_0 = \arg \min_{\forall \mathcal{E}} \langle \|\phi_0 - \mathcal{E} \mathbf{s}\|^2 \rangle_{\phi, n}, \quad (5.2.11)$$

where  $\mathcal{E}$  is the linear estimator operator. Analogously to the deterministic orthogonality principle the *orthogonality principle of statistical estimation* states that

optimal estimator error is statistically orthogonal to the measurements,

i.e., for our case

$$\langle (\mathcal{E}\mathbf{s} - \phi_0)\mathbf{s}^T \rangle_{\phi,n} = 0. \quad (5.2.12)$$

Solving Eq. (7.2.11) or its equivalent (7.2.12) yields

$$\tilde{\phi}_0 = \langle \mathbf{s}^T \phi \rangle_{\phi,n} \langle \mathbf{s} \mathbf{s}^T \rangle_{\phi,n}^{-1} \mathbf{s}. \quad (5.2.13)$$

The optimal estimation error is

$$\begin{aligned} \langle J_e \rangle_{\phi,n} &= \langle [\phi_0 - \tilde{\phi}_0, \phi_0 - \tilde{\phi}_0] \rangle_{\phi,n} \\ &= \langle [\phi_0 - \tilde{\phi}_0, \phi] \rangle_{\phi,n} \\ &= \langle [\phi_0, \phi_0] \rangle_{\phi,n} - \langle \mathbf{s}^T \phi_0 \rangle_{\phi,n} \langle \mathbf{s} \mathbf{s}^T \rangle_{\phi,n}^{-1} \langle \mathbf{s} \phi_0 \rangle_{\phi,n}, \end{aligned} \quad (5.2.14)$$

where Eqs. (7.2.12), (7.2.13) were used.

Comparison Eq. (7.2.13) with Eq. (7.2.9) reveals the fact that the statistical estimation and fitting problems have essentially the same structure. Indeed, Eq. (7.2.13) coincides with Eq. (7.2.9) for the controllable part of the wavefront after substitutions

$$\begin{aligned} \langle \mathbf{s} \phi_0(x, y) \rangle_{\phi,n} &\rightarrow \mathbf{f}(x, y), \text{ (estimation influence functions),} \\ \langle \mathbf{s} \mathbf{s}^T \rangle_{\phi,n} &\rightarrow [\mathbf{f}, \mathbf{f}^T], \text{ (estimation Gramm matrix),} \\ \mathbf{s} &\rightarrow [\mathbf{f}, \phi_0], \text{ (projection on measurements),} \\ \tilde{\phi}_0 &\rightarrow \hat{\phi}_0, \text{ (observable part of wavefront).} \end{aligned}$$

Thus, there exists another, “observable-unobservable”, orthogonal decomposition of the input wavefront (see Ref. [3] for the proof):

$$\phi_0(x, y) = \tilde{\phi}_0(x, y) + \bar{\phi}_0(x, y), \quad (5.2.15)$$

where

$$\tilde{\phi}_0 = \langle \mathbf{s}^T \phi_0 \rangle_{\phi,n} \langle \mathbf{s} \mathbf{s}^T \rangle_{\phi,n}^{-1} \mathcal{M} \phi = \mathcal{O} \phi, \quad (5.2.16)$$

$$\bar{\phi}_0 = \phi_0 - \mathcal{O} \phi. \quad (5.2.17)$$

Again, the observable part of the wavefront, the only part of interest for AO wavefront sensing, is finite-dimensional, and either  $\mathbf{s}$  or  $\mathbf{w} = \langle \mathbf{s} \mathbf{s}^T \rangle_{\phi,n}^{-1} \mathbf{s}$  can be naturally used as discrete representations of the  $\tilde{\phi}_0$ .

### 5.2.3 Joint estimation and fitting, separation principle

Now consider the problem of joint estimation and fitting, namely, given measurement  $\mathbf{s}$  and a set of influence functions  $\mathbf{f}(x, y)$  find the control commands  $\hat{\mathbf{c}}$  such that

$$\hat{\mathbf{c}} = \mathcal{R}\mathbf{s} = \arg \min_{\forall \mathcal{R}} \langle \|\phi_0 - \mathbf{f}^T \mathcal{R} \mathbf{s}\|^2 \rangle_{\phi,n}, \quad (5.2.18)$$

where  $\mathcal{R}$  is the estimator matrix creating linear mapping from the set of sensor measurements to the set of DM commands. Expanding the norm in Eq. (7.2.18) one gets

$$\begin{aligned} \|\phi_0 - \hat{\phi}\|^2 &= \|(\phi_0 - \tilde{\phi}_0) + (\tilde{\phi}_0 - \hat{\phi})\|^2 \\ &= \|\bar{\phi}_0\|^2 + 2[\bar{\phi}_0, \tilde{\phi}_0 - \mathbf{f}^T \mathcal{R} \mathbf{s}] + \|\tilde{\phi}_0 - \mathbf{f}^T \mathcal{R} \mathbf{s}\|^2, \\ \hat{\phi} &= \mathbf{f}^T \mathcal{R} \mathbf{s}. \end{aligned} \quad (5.2.19)$$

$\langle [\bar{\phi}_0, \tilde{\phi}_0 - \mathbf{f}^T \mathcal{R} \mathbf{s}] \rangle_{\phi,n} = 0$  for an optimal phase estimate  $\tilde{\phi}_0$  because of the orthogonality principle (7.2.12). Thus

$$\begin{aligned} \langle J \rangle_{\phi,n} &= \langle \|\phi - \hat{\phi}\|^2 \rangle_{\phi,n} \\ &= \langle \|\bar{\phi}_0\|^2 \rangle_{\phi,n} + \langle \|\tilde{\phi}_0 - \mathbf{f}^T \mathcal{R} \mathbf{s}\|^2 \rangle_{\phi,n}, \end{aligned} \quad (5.2.20)$$

which is known as the *separation principle of the quadratic control*. Eq. (7.2.20) shows that the overall error can be minimized in two independent steps:

1. Find the observable part of the target phase  $\tilde{\phi}_0$  from Eq. (7.2.13).
2. Since  $\tilde{\phi}_0$  is not a stochastic quantity, the  $\langle \rangle_{\phi,n}$  brackets can be dropped for the second term reducing its minimization to deterministic fitting of the actuator influence functions to the phase estimate according to Eq. (7.2.6).

Following this path, i.e. substituting Eq. (7.2.13) into Eq. (7.2.6), we get for the optimal reconstructor matrix

$$\mathcal{R} = [\mathbf{f}, \mathbf{f}^T]^\dagger [\mathbf{f}, \langle \mathbf{s}^T \phi_0 \rangle_{\phi,n}] \langle \mathbf{s} \mathbf{s}^T \rangle_{\phi,n}^{-1}. \quad (5.2.21)$$

The error for this reconstructor is

$$\langle \hat{J} \rangle_{\phi,n} = \langle \bar{\phi}_0 \rangle_{\phi,n} + \langle \tilde{\phi}_0 \rangle_{\phi,n}, \quad (5.2.22)$$

where the first term is the phase estimation error given by Eq. (7.2.14), second term is the fitting error of the observable phase to the influence functions and is given by Eq. (7.2.7) after substituting  $\tilde{\phi}_0$  instead of  $\phi_0$ .

#### 5.2.4 Estimator for projected wavefront

An modification of the phase estimation algorithm is needed for the situation when it is necessary to find an estimate of the input phase part extractable from  $\phi(x, y)$  by a projection operation

$$\phi_p(x, y) = \mathcal{P}(\phi_0(x, y)), \quad (5.2.23)$$

where  $\mathcal{P}$  is a linear *projection operator*. Examples of such an operator are the controllable/uncontrollable  $\mathcal{F}$ ,  $(\mathcal{I} - \mathcal{F})$  projectors discussed above, the high-pass and low-pass spatial filters that are an indispensable part of the GMT LTAO control strategy to be discussed later in this document.

The optimal minimum least squares estimator for  $\mathcal{P}(\phi_0)$  wavefront instead of  $\phi_0$  is derived from the minimization problem

$$\mathcal{E}_p = \arg \min_{\mathcal{E}} \langle |\mathcal{P}(\phi_0) - \mathcal{E} \mathbf{s}|^2 \rangle \quad (5.2.24)$$

or from the orthogonality principle

$$\langle (\mathcal{P}(\phi_0) - \mathcal{E}_p \mathbf{s}) \mathbf{s}^T \rangle = 0, \quad (5.2.25)$$

which, due to linearity of  $\mathcal{P}$ , trivially yealds

$$\mathcal{E}_p = \mathcal{P}(\mathcal{E}), \quad (5.2.26)$$

where  $\mathcal{E}$  is given by Eq. (7.2.13). Interesting, if Eq. (7.2.26) is used to find an optimal estimate of the controllable part  $\hat{\phi}_0$  of the input phase, Eq. (7.2.21) for the optimal joint reconstructor results.

#### 5.2.5 Information deficiency in the WFS model. Aliasing error.

TBD

#### 5.2.6 Dynamic and closed-loop control

The MMSE controller described above is an oversimplified version of a real AO control algorithm based on two fundamental simplifying assumptions:

- *Open-loop operation*: it is assumed that the sensor measures input signal in the exit pupil directly, without any correction elements in the optical path in front of the sensor. A real AO system rarely works in open-loop regime because of small dynamic range of the existing WFSs. The more practical *closed-loop* operation assumes that all the correction elements (DMs, tip/tilt mirrors, etc.) are located in front of sensors and the latter measure the difference between the input signal (turbulent wavefront) and its correction by DMs. In this case the input to the WFS is not  $\phi(x, y)$  but  $\delta\phi(x, y)$  and the input to controller is not  $\mathbf{s}$  but  $\delta\mathbf{s}$ , the *error signal*.

- *Non-dynamic* operation: it is assumed that signals propagate through the control system instantaneously and without temporal shape distortions. In reality, dynamic effects exist in the system. Two most important of them are: 1) signal delays due to data transfers, CCD exposure/readout time and controller computation time, 2) signal distortions due to finite temporal bandwidth of the correction mechanism actuators. The dynamic effects increase the residual error and may also lead to system instability in closed-loop regime. To introduce dynamic effects one has to consider all quantities to be time-dependent by adding  $n$  sub-index,  $n = 1, \dots, \infty$ , for discrete time.

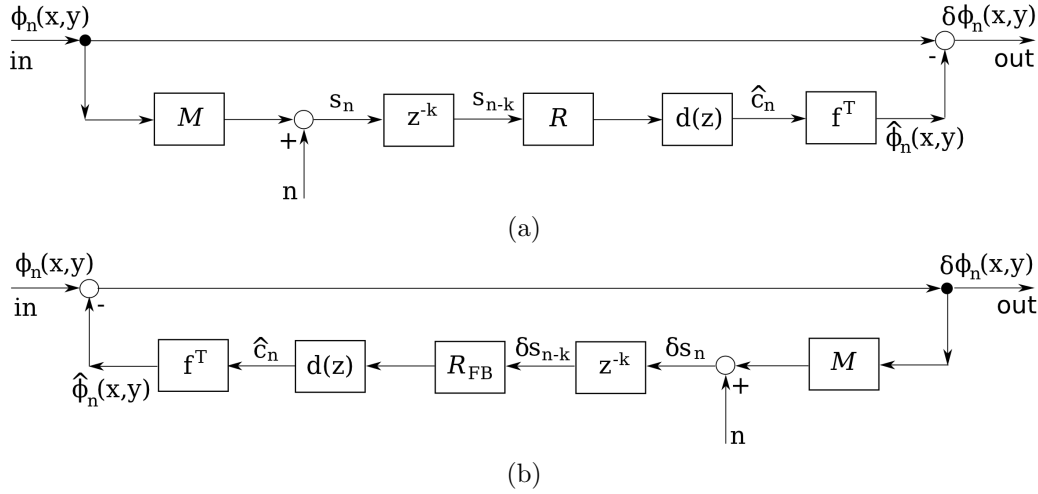


Figure 2: Open-loop (a) and closed-loop (b) AO controller block diagrams.

Simplified signal block diagrams for an AO system in open-loop and closed-loop configurations are shown on Fig. 2. The system dynamics are modeled by adding: 1)  $k$ -step signal delay element with  $z$ -domain transfer function  $z^{-k}$  to account for delays in sensor and controller; 2) a filter with  $z$ -domain transfer function (matrix)  $d(z)$  to account for the DM dynamic effects. It is possible to derive a relationship between the open-loop (or *feedforward*) reconstructor  $\mathcal{R}$  and the closed-loop (or *feedback*) one  $\mathcal{R}_{FB}$  by noticing that, to deliver the same output signal, it should be

$$\mathcal{R}s = \mathcal{R}_{FB}\delta s. \quad (5.2.27)$$

From the diagrams:

$$\begin{aligned} \delta s(z) &= s(z) - z^{-k}d(z)\mathcal{M}(f^T\mathcal{R}_{FB}\delta s(z)) \\ &= s(z) - z^{-k}d(z)\mathcal{D}\mathcal{R}_{FB}\delta s(z), \end{aligned} \quad (5.2.28)$$

where  $\mathcal{D} = \mathcal{M}(f^T)$  is the *poke matrix* relating action of each DM influence function on the WFS measurements. Substitution of Eq. (7.2.28) into Eq. (7.2.27) yields

$$\mathcal{R}_{FB} = \mathcal{R}(\mathcal{I} - z^{-1}d(z)\mathcal{R}\mathcal{D})^{-1}. \quad (5.2.29)$$

The transfers from input wavefront phase  $\phi(n)$  to the AO system residual phase error  $\delta\phi(n)$  (*error rejection transfer function*): for the feedforward and feedback controllers shown on Fig. 2 are:

$$(\phi \rightarrow \delta\phi)(z) = \mathcal{I} - z^{-k}d(z)\mathcal{D}\mathcal{R}; \quad (5.2.30)$$

$$(\phi \rightarrow \delta\phi)_{FB}(z) = (\mathcal{I} + z^{-k}d(z)\mathcal{D}\mathcal{R}_{FB})^{-1}. \quad (5.2.31)$$

The open-loop reconstructor  $\mathcal{R}$  can also be used directly in the *pseudo open-loop* (POL) setting of the closed-loop control when the open-loop measurement is approximately restored through an

internal model for the DM. In the case of linear internal model the approximate (pseudo) open-loop WFS measurement  $\hat{\mathbf{s}}$  is

$$\hat{\mathbf{s}} = \delta \mathbf{s} + \mathcal{D} \mathbf{c}. \quad (5.2.32)$$

Block diagram for a dynamic MMSE controller working in the POL regime is shown on Fig. 3. The integrator/corrector filter  $g(z)$  is used to produce the absolute DM commands from differential ones in a way ensuring system stability and dynamic error minimization.

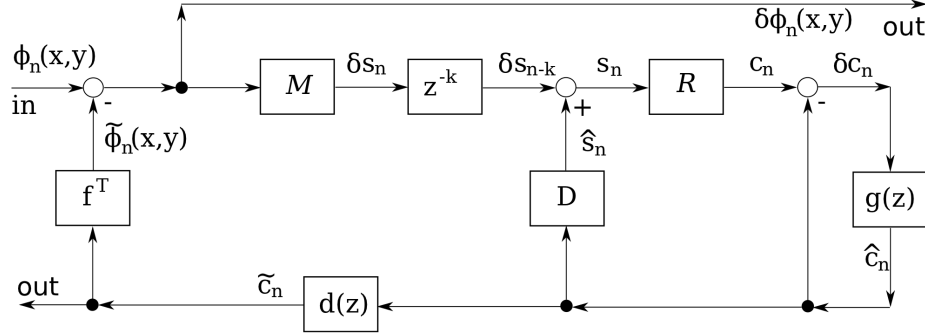


Figure 3: Pseudo Open-Loop MMSE controller block diagram.

The set of dynamic equations for the POL controller is:

$$\begin{aligned} & \text{(pseudo open-loop measurement)} \\ & \mathbf{s}(n) = \delta \mathbf{s}(n-k) + \hat{\mathbf{s}}(n); \end{aligned} \quad (5.2.33)$$

$$\begin{aligned} & \text{(pseudo open-loop command)} \\ & \mathbf{c}(n) = \mathcal{R} \mathbf{s}(n); \end{aligned} \quad (5.2.34)$$

$$\begin{aligned} & \text{(command increment)} \\ & \delta \mathbf{c} = \mathbf{c}(n) - \hat{\mathbf{c}}(n); \end{aligned} \quad (5.2.35)$$

$$\begin{aligned} & \text{(integrator/corrector state space equations, see Appendix 9)} \\ & \mathbf{x}^g(i+1) = \mathcal{A}^g \mathbf{x}^g(n) + \mathcal{B}^g \delta \mathbf{c}(n), \end{aligned} \quad (5.2.36)$$

$$\hat{\mathbf{c}}(n) = \mathcal{C}^g \mathbf{x}^g(n) + \mathcal{D}^g \delta \mathbf{c}(n); \quad (5.2.37)$$

$$\begin{aligned} & \text{(pseudo open-loop measurement estimate)} \\ & \hat{\mathbf{s}}(n) = \mathcal{D} \hat{\mathbf{c}}(n). \end{aligned} \quad (5.2.38)$$

Two important transfer functions (matrices) can be derived from the Fig. 3 diagram: 1) the transfer from WFS output  $\delta \mathbf{s}(n)$  to controller output  $\hat{\mathbf{c}}(n)$  (*controller transfer function*):

$$(\delta \mathbf{s} \rightarrow \hat{\mathbf{c}})_{POL}(z) = z^{-2} g(z) [\mathcal{I} + g(z)(\mathcal{I} - \mathcal{R} \mathcal{D})]^{-1} \mathcal{R}, \quad (5.2.39)$$

and 2) the error rejection transfer function:

$$(\phi \rightarrow \delta \phi)_{POL}(z) = [\mathcal{I} + d(z) \mathbf{f}^T (\delta \mathbf{s} \rightarrow \hat{\mathbf{c}})_{POL}(z) \mathcal{D}]^{-1}. \quad (5.2.40)$$

Being formally equivalent, feedforward, feedback and POL controllers have different stability and error propagation properties.

### 5.3 Tomographic MMSE reconstructor

A generalization of the single-conjugate AO control is the *star-oriented tomography*.

## 5.4 GMT LTAO sub-systems

According to the *split control concept* the entire GMT LTAO system can be viewed as a set of weakly interacting control sub-systems (feedback loops, see Fig. TBD):

1. The *ASM high order LGS-based* (ASM HO LGS) control loop intended to reject high spatial order atmospheric/telescope aberrations and using the LGS return for WFS measurements. This channel has the following features:
  - This channel works in closed-loop behind ASM.
  - Target is  $\phi_{Sc}$  is the wavefront from a scientific object.
  - Reference is  $\phi_{LGS}$  is the wavefront from 6 LGSs.
  - The control commands generated in this channel are sent to the ASM.
  - The wavefront sensors for this channel are the 6 LGS WFSs.
  - The sampling rate is the one of the LGS WFSs.
2. The *ASM low order NGS-based* (ASM LO NGS) or “truth” control loop is used to provide low order ASM correction, which is impossible to determine from the LGSs. Another possible use of the LO NGS WFS is to sense the primary segment differential pistons. This channel has the following features:
  - This channel works in closed-loop behind ASM and OI DM.
  - Target is the wavefront  $\phi_{Sc}$  from a scientific object.
  - Reference is the wavefront  $\phi_{NGS}$  from one NGS.
  - The control commands generated by this channel are sent to ASM.
  - The wavefront sensor for this channel is the LO NGS WFS (“truth sensor”).
  - The sampling rate is the one of the LO NGS WFS.
3. The *ASM tip/tilt NGS-based* (ASM TT NGS) control loop intended to sense and correct the wavefront tip/tilt in the scientific object direction using a natural guide star. This channel has the following features:
  - This channel works in closed-loop behind ASM and OI DM.
  - Target is the wavefront  $\phi_{Sc}$  from a scientific object.
  - Reference is the wavefront  $\phi_{NGS}$  from one NGS.
  - The control commands generated in this channel are sent to the ASM.
  - The wavefront sensor for this channel is a quad-cell tip/tilt NGS (TT NGS) WFS.
  - The sampling rate is the one of the TT WFS.
4. The *OI DM high order LGS-based* (OI DM HO LGS) control loop is for correcting the NGS wavefront by the OI DM in order to improve performance of the NGS TT channel. This channel has the following features:
  - This channel works in closed-loop behind ASM.
  - Target is the wavefront  $\phi_{NGS}$  from a NGS.
  - Reference is the wavefront  $\phi_{LGS}$  from 6 LGSs.
  - The control commands generated in this channel are sent to OI DM.
  - The wavefront sensors for this channel are the 6 LGS WFSs.
  - The control algorithm is closed-loop with respect to the ASM but open-loop with respect to OI DM.

- The sampling rate is the one of the LGS WFSs.
5. The *OI DM low order NGS-based* (OI DM LO NGS) control loop is to provide the low order OI DM correction, which is not possible to determine from the LGSs. This channel has the following features:
- This channel works in closed-loop behind ASM and OI DM.
  - Target is the wavefront  $\phi_{NGS}$  from a NGS.
  - Reference is the wavefront  $\phi_{NGS}$  from the same NGS.
  - The control commands generated by this channel are sent to OI DM.
  - The wavefront sensor for this channel is the LO NGS WFS.
  - The sampling rate is the one of the LO NGS WFS.

One has also to mention some auxiliary control channels used for or together with LTAO. They are not based on the standard AO control and use other control approaches.

1. *LGS focus stabilization subsystem* is used for adjusting the LGS WFS module focal plane to follow slow LGS position changes in the sky. This channel has the following features:
  - The feedback signal is the global focus mode extracted from the 6 LGS WFS measurements.
  - The control is applied to a servo actuator moving the whole LGS WFS module to adjust to the focus. The controller needs to be optimized to the (actuator + LGS module) dynamics.
2. *LGS pupil de-rotation subsystem* is used for compensation of the exit pupil rotation on the LGS module induced by changes in the telescope pointing. This channel has the following features:
  - The feedback signal for this channel is the correlated part of the LGS WFS spot motions.
  - The control is applied to a servo actuator rotating the whole LGS WFS module to adjust to the pupil rotation.
3. *OI WFS acquisition/image stabilization subsystem* is used find the NGS in the telescope field-of-view, to point the light from an NGS to the OI WFS detectors and stabilize it. This channel has the following features:
  - An acquisition camera is used to provide a signal to the controller.
  - The control is applied to a two degree-of-freedom actuator attached to the acquisition flat mirror located inside OI WFS module.
  - The acquisition camera and mirror work in closed-loop regime behind ASM and OI DM.
4. *GMT phasing subsystem* is an *active optics* system that keeps the telescope aligned, phased and shape-stabilized.

The auxiliary control sub-systems do not directly participate in the AO correction but the errors in these systems become the additional error inputs for the main AO controllers thus upsetting indirectly the AO system performance.



**5.4.1 ASM HO LGS controller algorithm**

**5.4.2 ASM LO NGS controller algorithm**

**5.4.3 ASM TT NGS controller algorithm**

**5.4.4 OI DM HO LGS controller algorithm**

**5.4.5 OI DM LO NGS controller algorithm**

**5.5 GMT LTAO system fusion**

TBD

**5.6 GMT LTAO system dynamic analysis**

TBD

**5.7 GMT LTAO system error and robustness analysis**

TBD

## 6 Appendix: Matrix derivatives

Derivative of linear matrix functional

$$p^T F z$$

with respect to matrix  $F$  is computed as follows:

1. Write the functional in element-wise form:

$$f = p^T F z = \sum_i \sum_j p_i F_{ij} z_j.$$

2. Differentiate with respect to  $F_{ij}$ :

$$\frac{\partial f}{\partial F_{ij}} = p_i z_j.$$

3. Thus

$$\frac{\partial}{\partial F}(p^T F z) = p z^T.$$

Derivative of quadratic matrix functional

$$z^T F^T A F z,$$

where  $A$  is symmetric real valued matrix, with respect to matrix  $F$  is computed as follows:

1. Write the functional in element-wise form:

$$f = z^T F^T A F z = \sum_{i=1}^m \sum_{l=1}^n \sum_{j=1}^m \sum_{k=1}^n F_{il} F_{jk} A_{ij} z_l z_k$$

2. Most conveniently, by writing down the above equation for a case of small matrix size, say, 2x2, find by inspection that

$$\frac{\partial}{\partial F}(z^T F^T A F z) = 2 A F z z^T.$$

## 7 Appendix: Basic discrete-time digital filter theory

Here the basic formulas for the digital linear filter theory are given.

*Definition:* a time-invariant, single-input-single-output (SISO), order  $N$  discrete-time linear digital filter is given by a linear, order- $N$  difference equation with constant coefficients:

$$y(i) = \sum_{k=0}^N b_k u(i-k) - \sum_{k=1}^N a_k y(i-k), \quad i = 0, \dots \quad (7.0.1)$$

where  $i$  is *discrete time*,  $u(i)$  is the *input sequence*,  $y(i)$  is the *output sequence*. The filter in Eq. (9.0.1) is called *causal* because  $y(i)$  does not depend on time instances  $i+1$  and on. Applying  $z$ -transform to Eq. (9.0.1) one gets:

$$y(z)(1 + \sum_{k=1}^N a_k z^{-k}) = u(z) \sum_{k=0}^N b_k z^{-k}.$$

from where the *transfer function* is:

$$H(z) = \frac{y(z)}{u(z)} = b_0 + \frac{\sum_{k=1}^N \beta_k b_k z^{-k}}{1 + \sum_{k=1}^N a_k z^{-k}}, \quad (7.0.2)$$

$$\beta_k = b_k - b_0 a_k.$$

The canonical state-space model

$$\mathbf{x}(i+1) = \mathcal{A}\mathbf{x}(i) + \mathcal{B}\mathbf{u}(i), \quad (7.0.3)$$

$$\mathbf{y}(i) = \mathcal{C}\mathbf{x}(i) + \mathcal{D}\mathbf{u}(i)$$

describes the filter in terms of its internal state  $\mathbf{x}(i)$  dynamics. The first equation is the *state dynamics equation*, the second is the *measurement equation*. The state space model parameters for the filter are easily derivable from Eq. (9.0.2):

$$\mathbf{u}(i) = [u(i)], \quad (7.0.4)$$

$$\mathbf{y}(i) = [y(i)],$$

$$\mathcal{A} = \begin{bmatrix} -a_1 & -a_2 & \cdots & -a_{N-1} & -a_N \\ 1 & 0 & \cdots & 0 & 0 \\ 0 & 1 & \cdots & 0 & 0 \\ \vdots & \vdots & \ddots & \vdots & \vdots \\ 0 & 0 & \cdots & 1 & 0 \end{bmatrix}$$

$$\mathcal{B} = [1 \cdots 0]^T,$$

$$\mathcal{C} = [\beta_1 \cdots \beta_N],$$

$$\mathcal{D} = [b_0].$$

## 8 Bibliography

### References

- [1] O. Lardiere, R. Conan, R. Clare, C. Bradley, N. Hubin, “Performance comparison of centroiding algorithms for laser guide star wavefront sensing with extremely large telescopes,” *Appl. Opt.*, **49**, G78-G94 (2010).
- [2] D. M. Wiberg, C. E. Max, and D. T. Gavel, “A spatial non-dynamic LQG controller: Part 1, Application to adaptive optics,” in *Proceedings of the 2004 IEEE Conference on Decision and Control* (IEEE, 2004), pp. 3326 - 3332.
- [3] D. M. Wiberg, C. E. Max, and D. T. Gavel, “A spatial non-dynamic LQG controller: Part 2, Theory,” in *Proceedings of the 2004 IEEE Conference on Decision and Control* (IEEE, 2004), pp. 3333 - 3338.
- [4] D. M. Wiberg, C. E. Max, and D. T. Gavel, “Geometric view of adaptive optics control,” *JOSA*, **22**, pp. 870 - 880 (2004).

# Index

affine transform, 6  
aperture, 16  
ASM high order LGS-based control loop, 22  
ASM low order NGS-based control loop, 22  
ASM tip/tilt NGS-based control loop, 22  
  
causal filter, 26  
Center of Gravity centroid, 11, 12  
controllable part, 17  
controllable subspace, 17  
controller transfer function, 21  
Correlation centroid, 11  
  
discrete time, 26  
DM fitting, 16  
  
error rejection transfer function, 21  
error signal, 20  
  
fitting error, 17  
  
GMT phasing subsystem, 24  
  
input sequence, 26  
  
LGS focus stabilization subsystem, 23  
LGS pupil de-rotation subsystem, 23  
  
measurement equation, 16, 26  
measurement operator, 16  
Minimum Mean Square Error, 16  
  
non-dynamic operation, 20  
  
OI DM high order LGS-based control loop, 23  
OI DM low order NGS-based control loop, 23  
OI WFS acquisition/image stabilization subsystem, 23  
open-loop operation, 20  
orthogonality principle, 17  
output sequence, 26  
  
phase estimation, 16  
phase screen, 7  
poke matrix, 21  
projection operator, 19  
pseudo open-loop, 21  
  
quad cell, 11  
quadratic cost, 16  
  
ray, 7  
reference image, 11  
  
separation principle, 19  
split control concept, 22  
star-oriented tomography, 22  
state dynamics equation, 26  
  
transfer function, 26  
  
uncontrollable part, 17  
uncontrollable subspace, 17  
  
wavefront, 7  
Weighted Center of Gravity centroid, 11